Metal complexes of tetradentate and pentadentate N-o-hydroxybenzamido-meso-tetraphenylporphyrin ligand: M(N-NCO(o-OH)C6H4-tpp) (M = Zn2+, Ni2+, Cu2+) and M′ (N-NCO(o-O) C6H4-tpp) (M...

ARTICLE *in* POLYHEDRON · DECEMBER 2009

Impact Factor: 2.01 · DOI: 10.1016/j.poly.2009.09.009

Polyhedron 28 (2009) 3907–3914

Contents lists available at ScienceDirect

Polyhedron

journal homepage: www.elsevier.com/locate/poly

Metal complexes of tetradentate and pentadentate *N*-*o*-hydroxybenzamido-*meso*-tetraphenylporphyrin ligand: M(*N*-NCO(*o*-OH)C_6H_4-tpp) (M = Zn^{2+}, Ni^{2+}, Cu^{2+}) and M′(*N*-NCO(*o*-O) C_6H_4-tpp) (M′ = Mn^{3+}) (tpp = 5, 10, 15, 20-tetraphenylporphyrinate)

Ting-Yuan Chien [a], Hua-Yu Hsieh [a], Chun-Yi Chen [a], Jyh-Horung Chen [a,*], Shin-Shin Wang [b], Jo-Yu Tung [c,*]

[a] Department of Chemistry, National Chung Hsing University, Taichung 40227, Taiwan
[b] Material Chemical Laboratories ITRI, Hsin-Chu 300, Taiwan
[c] Department of Occupational Safety and Health, Chung Hwai University of Medical Technology, Taiwan

ARTICLE INFO

Article history:
Received 24 August 2009
Accepted 1 September 2009
Available online 18 September 2009

Keywords:
Manganese porphyrin
Zero field splitting
EPR spectra
Magnetic susceptibility

ABSTRACT

The crystal structures of *N*-*o*-hydroxybenzimido-*meso*-tetraphenylporphyrinatozinc(II) toluene solvate [Zn(*N*-NCO(*o*-OH)C_6H_4-tpp)·$C_6H_5CH_3$; **4**·$C_6H_5CH_3$], *N*-*o*-hydroxybenzimido-*meso*-tetraphenylporphyrinatonickel(II) chloroform solvate [Ni(*N*-NCO(*o*-OH)C_6H_4-tpp)·0.6$CHCl_3$; **5**·0.6 $CHCl_3$], *N*-*o*-hydroxybenzimido-*meso*-tetraphenylporphyrinatocopper(II) toluene solvate [Cu(*N*-NCO(*o*-OH)C_6H_4-tpp)·$C_6H_5CH_3$; **6**·$C_6H_5CH_3$] and *N*-*o*-oxido-benzimido-*meso*-tetraphenylporphyrinato(-κ^4,N^1,N^2,N^3,N^5,κO^2) manganese (III) methylene chloride·methanol solvate [Mn(N-NCO(*o*-O)C_6H_4-tpp)·CH_2Cl_2·MeOH; **8**·CH_2Cl_2·MeOH] were established. The coordination sphere around Zn^{2+} ion in **4**·$C_6H_5CH_3$, (or Ni^{2+} ion in **5**·0.6 $CHCl_3$ or Cu^{2+} ion in **6**·$C_6H_5CH_3$) is a distorted square planar (DSP) whereas for Mn^{3+} in **8**·CH_2Cl_2·MeOH, it is a distorted trigonal bipyramid (DTBP) with O(1), N(1) and N(3) lying in the equatorial plane for **8**·CH_2Cl_2·MeOH. The g value of 8.27 measured from the parallel polarization of X-band EPR spectra at 293 K is consistent with the high-spin mononuclear manganese(III) (S = 2) in **8**. The magnitude of axial (D) zero-field splitting (ZFS) for the mononuclear Mn(III) in **8** was determined approximately as 3.0 cm^{-1} by the paramagnetic susceptibility measurements and conventional EPR spectroscopy.

1. Introduction

Previously, we reported the two-stage formation of (*N*-*o*-chlorobenzamido-*meso*-tetraphenylporphyrinato)zinc (II) (**1**) [1]. Compound **1** is a zinc complex of *N*-NHCO(*o*-Cl)C_6H_4-Htpp (**2**) (Scheme 1). In **2**, when the ortho chlorine is replaced by hydroxyl ligand, a new free aminated porphyrin is formed namely *N*-*o*-hydroxy benzamido-*meso*-tetraphenylporphyrin [*N*-NHCO(*o*-OH)C_6H_4-Htpp; **3**] (Fig. 1a) [2]. Compound **3** is a N-substituted porphyrin [3]. A carbonyl group in the ortho position of **3** shifts the phenolic proton absorption to the range of about δ 12.0–δ 10.0 ppm in CD_2Cl_2 because of intramolecular hydrogen bonding [4]. Thus, compound **3** shows a peak at about δ 11.95 in CD_2Cl_2 at 20 °C almost completely invariant with the concentration. It is worth to note the structure of porphrin ligand **3** as the presence of hydroxyl ligands plays a role in somewhat artificially increasing the coordination-number when **3** is coordinated to the metal ions. We explored coordination properties of *N*-*o*-hydroxy benzamido-*meso*-tetraphenylporphyrin. A thorough literature review reveals that there is no report on the metal complex of **3**. Depending on the metal ion choice two principal structural motifs have been detected. In the first case [copper(II), zinc(II), Ni(II)] the N-substituted porphyrin acts as tetradentate macrocycle using three pyrrolic and one amidate nitrogen (Scheme 2).The trivalent metal ions [gallium(III), manganese(III)] preserve the pattern of the equatorial coordination but in addition the apical position is occupied by the phenoxy moiety of the N-substituent (Scheme 2).

The complexation of Zn^{2+}, Ni^{2+} and Cu^{2+} classified as divalent B acids into **3** retains the intramolecular hydrogen bonding and

* Corresponding authors. Tel.: +886 4 228 40411x612; fax: +886 4 228 62547 (J.-H. Chen), tel.: +886 6 267 4567x815; fax: +886 6 289 4028 (J.-Y. Tung).
E-mail addresses: JyhHChen@dragon.nchu.edu.tw (J.-H. Chen), joyuting@mail.hwai.edu.tw (J.-Y. Tung).

0277-5387/$ - see front matter Crown Copyright © 2009 Published by Elsevier Ltd. All rights reserved.
doi:10.1016/j.poly.2009.09.009

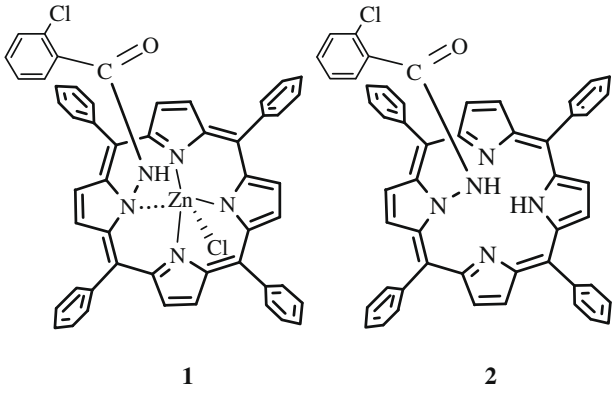

Scheme 1.

forms four-coordinate zinc(II) (**4**), nickel(II) (**5**) and copper(II) (**6**) complexes (Scheme 2) [5–7].[1]

Moreover for Ga^{3+} and Mn^{3+} with the coordination-number (CN) = 5 and a higher *Z* are trivalent E acids [6]. A strongly attractive electrostatic interaction between the gallium [Ga^{3+}] (or Mn^{3+}) and oxygen atom [i.e., $O(2)^-$] in **7** [or $O(1)^-$ in **8**] destroy intramolecular hydrogen bonding O(1)···H(2A) in **3** and rotate (*o*-O)BA ligand along the C(45)–C(46) bond in **7** [or C(50)–C(51) bond in **8**] and finally stabilize the five-coordinate gallium(III) (**7**) [or manganese (III) (**8**)] complexes (Scheme 2) [2]. The lack of study on metal complexes of ligand **3** prompted us to undertake the synthesis and structural investigations of the zinc(II), nickel(II), copper (II) and manganese(III) complexes. In this paper, we describe the X-ray structural investigation on the metallation of **3** leading to the zinc complex of *N*-*o*-hydroxybenzimido-*meso*-tetraphenylporphyrinatozinc(II) toluene solvate [Zn(*N*-NCO(*o*-OH)C_6H_4-tpp)·$C_6H_5CH_3$; **4**·$C_6H_5CH_3$], nickel complex of *N*-*o*-*hydroxybenzimido*-*meso*-tetraphenylporphyrinatonickel(II) chloroform solvate [Ni(*N*-NCO(*o*-OH)C_6H_4-tpp)·0.6 $CHCl_3$; **5**·0.6 $CHCl_3$], copper complex of *N*-*o*-hydroxybenzimido-*meso*-tetraphenylporphyrinatocopper(II) toluene solvate [Cu(*N*-NCO(*o*-OH)C_6H_4-tpp)·$C_6H_5CH_3$; **6**·$C_6H_5CH_3$] and manganese(III) complex of *N*-*o*-oxido-benzimido-*meso*-tetraphenylporphyrinato -(-κ^4,N^1,N^2,N^3,N^5,κO^2) manganese (III) methylene chloride·methanol solvate [Mn(*N*-NCO(*o*-O)C_6H_4-tpp)·CH_2Cl_2·MeOH; **8**·CH_2Cl_2·MeOH]. The reported diamagnetic compound **7** is used as a diamagnetic correction for paramagnetic complex **8** in the solid-state magnetic susceptibility measurements [2,7]. We also focus on the details of manganese (III) electronic structure of **8**. Studies of temperature dependence of magnetic susceptibility and effective moment show that S = 2, is the ground state for high-spin mononuclear Mn^{3+} in **8** at 20 °C. Application of the Bleaney–Bowers equation permits evaluation of D and an average *g* value for powder samples of **8** [8].

[1] Zhang suggested a scale for the Lewis acid strengths that has been calculated from the dual parameter equation $Z = \frac{z}{r_k^2} - 7.7\chi_z + 8.0$ [5,6]. One parameter, $\frac{z}{r_k^2} = P =$ (polarizing power), where *z* is the charge number of the atomic core and r_k is the ionic radius, is related to electrostatic force. Another parameter, the electronegativity of elements in valence states, χ_z is related to covalent bond strength. The metal ions in which there is clear dominance by the electrostatic force $\frac{z}{r_k^2}$ have *Z* values higher than 0.66. They call these acids large electrostatic acids or simply E acids. The metal ions in which there is clear dominance by the electronegativity χ_z, i.e. with a large covalent property and have *Z* values lower than zero. They call these acids large covalent acids, or simply C acids [6]. The metal ions lying between E and C acids and having *Z* values higher than zero and lower than 0.66 are border acids, or simply B acids. Although scales by Zhang which have been less widely used [6], we tried to coordinate the metal ions with B and E acids to ligand **3** and figure out the structural parameters that control the formation of these four-coordinate and five-coordinate porphyrin metal complexes. The cations were selected on the basis of differences in *Z* of the metal cations. The cations selected were Cu^{2+} (B acid), Ni^{2+} (B acid), Zn^{2+} (B acid), Ga^{3+} (E acid) and Mn^{3+} (E acid), for which *Z* = 0.177, 0.293, 0.656, 1.167 and 1.698, respectively.

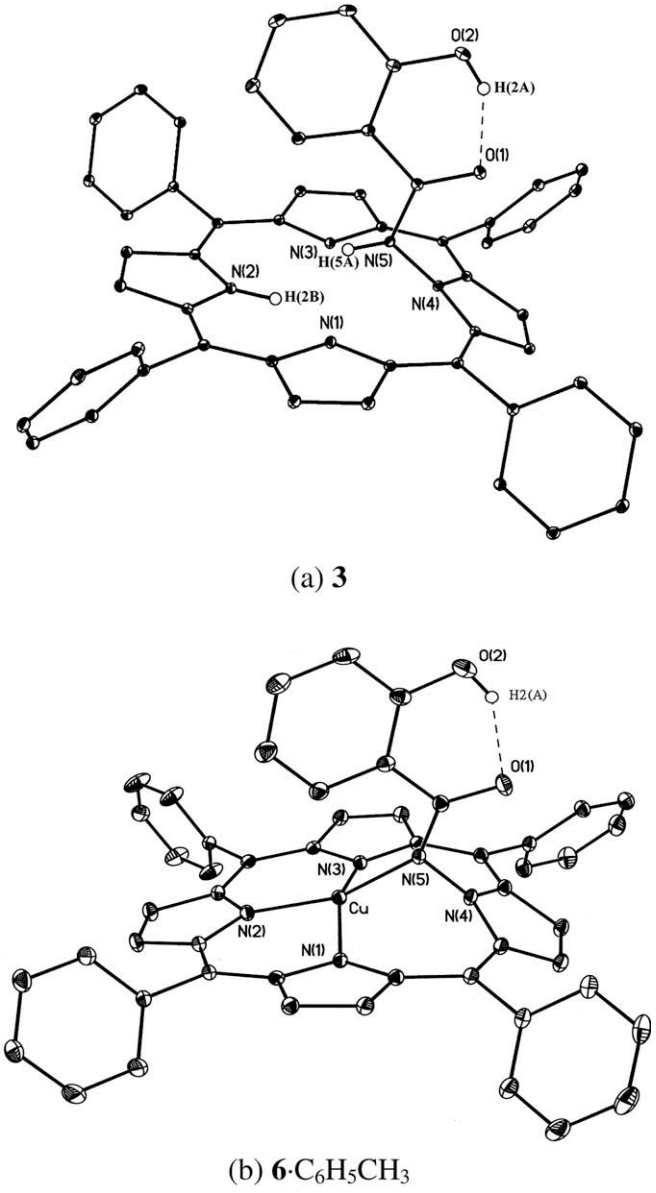

Fig. 1. Molecular configuration and atom-labeling scheme for (a) **3** [2] and (b) [Cu(*N*-NCO(*o*-OH)C_6H_4-tpp)·$C_6H_5CH_3$; **6**·$C_6H_5CH_3$], with 30% thermal ellipsoids. Hydrogen atoms and solvent $C_6H_5CH_3$ for **6**·$C_6H_5CH_3$ are omitted for clarity.

2. Experimental

2.1. Zn(*N*-NCO(*o*-OH)C_6H_4-tpp) (*4*)

A mixture of **3** (0.051 g, 0.068 mmol) in CH_2Cl_2 (20 cm^3) and $Zn(OAc)_2·2H_2O$ (0.05 g, 0.228 mmol) in MeOH (5 cm^3) was refluxed at 60 °C for 3 h. After concentration, the residue was dissolved in CH_2Cl_2 and dried with anhydrous Na_2SO_4 and filtered [2,3]. The filtrate was concentrated yielding purple solid which was again dissolved in CH_2Cl_2 and layered with MeOH to get purple solid of **4**·$C_6H_5CH_3$ (0.043 g, 0.053 mmol, 78%). Compound **4**·$C_6H_5CH_3$ was dissolved in toluene and layered with hexane to afford purple crystals for single-crystal X-ray analysis. ^{1}H NMR (599.95 MHz, CD_2Cl_2, 20 °C): δ 11.49 [s ($\Delta\nu_{1/2}$ = 1 Hz, OH], where (*o*-OH)BA = *o*-hydroxybenzamido ligand; 9.09 [d, H_β(2,13), $^{3J(H-H)}$ = 4.8 Hz]; 8.92 [s, H_β(7,8)]; 8.92 [d, H_β(3,12), ^3J(H–H) = 3.6 Hz]; 7.79 [s, H_β(17,18)]; 8.40 [d, *o*-H(22,32), ^3J(H–H) = 6.6 Hz]; 8.11 [d, *o*-H(26,28), ^3J(H–H) = 7.2 Hz];11.49 [s, (*o*-OH)BA-OH]; 6.16 [t, (*o*-OH)BA-Ph-H_4,

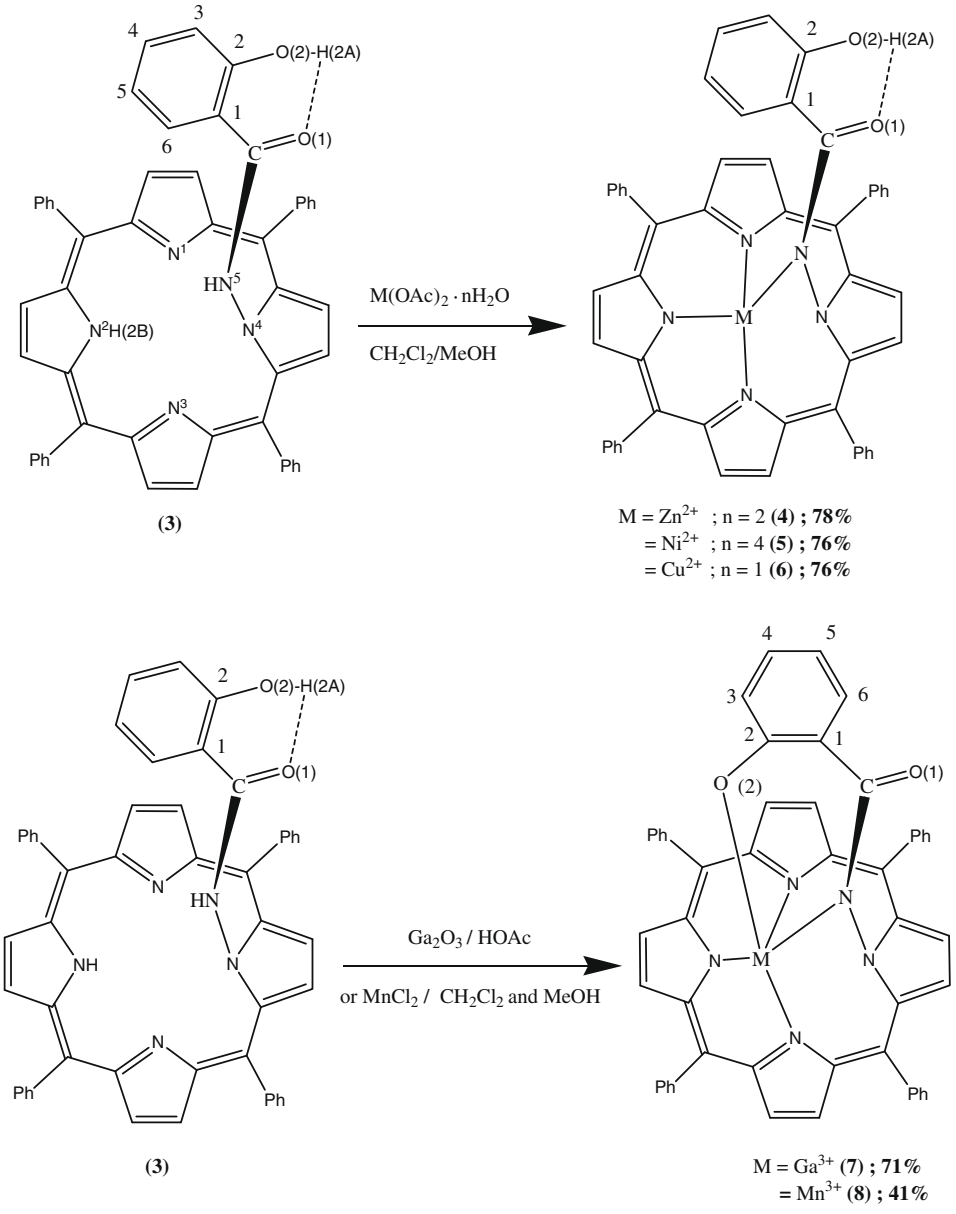

Scheme 2.

^3J(H–H) = 8.4 Hz]; 5.79 [d, (*o*-OH)BA-Ph-H$_3$, ^3J(H–H) = 8.4 Hz]; 4.69 [t, (*o*-OH)BA-Ph-H$_5$, ^3J(H–H) = 7.7 Hz]; 1.47 [d, (*o*-OH)BA-Ph-H$_6$, ^3J(H–H) = 8.1 Hz]. MS (FAB): $(M)^+$ 812 (calcd for $C_{51}H_{33}N_5O_2Zn$: 813). UV–vis [λ, nm (10^{-3} ε, M^{-1} cm^{-1})] in CH_2Cl_2: 605 (12.7), 437 (284.2).

2.2. Ni(*N*-NCO(*o*-OH)C_6H_4-tpp) (**5**)

Compound **5**·0.6$CHCl_3$ in 76% yield was prepared in the same way as described for Zn(*N*-N(*o*-OH)C_6H_4-tpp) (4·$C_6H_5CH_3$) using $Ni(OAc)_2{\cdot}4H_2O$. Compound **5**·0.6$CHCl_3$ was dissolved in $CHCl_3$ and layered with MeOH to afford purple crystals for single-crystal X-ray analysis. ^{1}H NMR (599.95 MHz, CD_2Cl_2, 20 °C): δ 11.18 [s ($\Delta\nu_{1/2}$ = 2 Hz, OH]; 8.94 [d, H$_\beta$(2,13), ^3J(H–H) = 5.4 Hz]; 8.81 [s, H$_\beta$(7,8)]; 8.67 [d, H$_\beta$(3,12), ^3J(H–H) = 4.8 Hz]; 7.63 [s, H$_\beta$(17,18)]; 8.21 [d, *o*-H(26,32), ^3J(H–H) = 6.6 Hz]; 8.11 [d, *o*-H(22,28), ^3J(H–H) = 7.8 Hz]; 6.34 [t, (*o*-OH)BA-Ph-H$_4$, ^3J(H–H) = 6.9 Hz]; 5.94 [d, (*o*-OH)BA-Ph-H$_3$, ^3J(H–H) = 7.2 Hz]; 5.53 [d, (*o*-OH)BA-Ph-H$_6$, ^3J(H–H) = 7.8 Hz]; 5.09 [t, (*o*-OH)BA-Ph-H$_5$, ^3J(H–H) = 8.1 Hz]. MS (FAB): $(M)^+$ 806 (calcd for $C_{51}H_{33}N_5O_2Ni$: 806). UV–vis [λ, nm (10^{-3} ε, M^{-1} cm^{-1})] in CH_2Cl_2: 558 (12.5), 422 (128.4).

2.3. Cu(*N*-NCO(*o*-OH)C_6H_4-tpp) (**6**)

Compound **6**·$C_6H_5CH_3$ in 76% yield was prepared in the same way as described for Zn(*N*-N(*o*-OH)C_6H_4-tpp)·$C_6H_5CH_3$ (**4**·$C_6H_5CH_3$) using $Cu(OAc)_2{\cdot}H_2O$ with a reaction time of 60 min. Compound **6**·$C_6H_5CH_3$ was dissolved in toluene and layered with hexane to afford a purple crystals for single-crystal X-ray analysis. MS (FAB): $(M)^+$ 810 (calcd for $C_{51}H_{33}N_5O_2Cu$: 811). UV–vis [λ, nm (10^{-3} ε, M^{-1} cm^{-1})] in CH_2Cl_2: 592 (10.7), 563 (10.0), 429 (225.5).

2.4. Mn(*N*-NCO(*o*-O) C_6H_4-tpp) (**8**)

A mixture of **3** (0.051 g, 0.068 mmol) in CH_2Cl_2 (50 cm^3) and $MnCl_2$ (0.025 g, 0.20 mmol) in MeOH (50 cm^3) was refluxed in pyridine (2 cm^3) at 60 °C for 12 h. After concentrating, the residue was dissolved in a suitable amount of CH_2Cl_2, dried over anhydrous

Table 1
Crystal data for **4**·$C_6H_5CH_3$, **5**·0.6$CHCl_3$, **6**·$C_6H_5CH_3$ and **8**·CH_2Cl_2·MeOH.

Compound	**4**·$C_6H_5CH_3$	**5**·0.6$CHCl_3$	**6**·$C_6H_5CH_3$	**8**·CH_2Cl_2·MeOH
Empirical formula	$C_{58}H_{41}N_5O_2Zn$	$C_{51.60}H_{33.60}Cl_{1.80}N_5NiO_2$	$C_{58}H_{33}CuN_5O_2$	$C_{53}H_{38}Cl_2MnN_5O_3$
Formula weight	905.33	878.14	895.44	918.72
Space group	$P2_1/c$	$P2_1/c$	$P2_1/c$	$P\bar{1}$
Crystal system	monoclinic	monoclinic	monoclinic	triclinic
a (Å)	13.7541(10)	14.580(3)	13.7432(8)	11.2537(4)
b (Å)	17.5633(13)	11.757(3)	17.5994(10)	13.1671(5)
c (Å)	18.8776(14)	26.462(6)	18.8654(11)	14.9143(5)
α (°)	90	90	90	80.820(3)
β (°)	98.3240(10)	103.068(4)	98.2840(10)	84.453(3)
γ (°)	90	90	90	83.439(3)
V (Å^3)	4512.2(6)	4418.6(18)	4515.4(5)	2160.44(13)
Z	4	4	4	2
F(0 0 0)	1880	1811.2	1844	948
D_{calcd}, (g cm^{-3})	1.333	1.320	1.317	1.412
μ(Mo K$_\alpha$), (mm^{-1})	0.595	0.595	0.534	0.482
S	1.209	1.119	1.338	1.283
Crystal size, (mm)	0.26 × 0.18 × 0.10	0.25 × 0.15 × 0.10	0.27 × 0.16 × 0.09	0.27 × 0.12 × 0.05
θ (°)	26.02	28.26	26.03	29.18
T (K)	293(2)	293(2)	293(2)	100(2)
Number of reflections measured	8879	10 950	8897	8095
Number of reflections observed	6637	7928	6408	10 220
R_1[a]	0.0544	0.0789	0.0622	0.0476
wR_2[b]	0.1648	0.2631	0.1842	0.1404

[a] $R_1 = [\sum||F_o| - |F_c||/\sum|F_o|]$.
[b] $wR_2 = [\sum w(F_o^2 - F_c^2)^2/\sum w(F_o^2)^2]^{1/2}$.

Na_2SO_4 and filtered. The filtrate was concentrated yielding pure solid which was again dissolved in CH_2Cl_2 and layered with MeOH [CH_2Cl_2:MeOH = 1:1 (v/v)] to get purple solid of **8** (0.025 g, 0.028 mmol, 41%). Compound **8** was redissolved in CH_2Cl_2 and layered with MeOH to afford purple crystals for single-crystal X-ray analysis. MS (FAB): $(M)^+$ 802 (calcd for $C_{51}H_{32}MnN_5O_2$). UV–vis [λ, nm (10^{-3} ε, M^{-1} cm^{-1})] in CH_2Cl_2: 641 (3.85), 608 (5.14), 464 (28.4), 423 (42.3). *Anal.* Calc. for $C_{51}H_{32}MnN_5O_2$: C, 76.40; H, 4.02; N, 8.73. Found: C, 75.94; H, 4.04; N, 8.34%.

2.5. Magnetic susceptibility measurements

The solid-state magnetic susceptibilities were measured under helium on a Quantum Design MPMS5 SQUID susceptometer from 2 to 300 K at a field of 5 kG. The sample was held in a Kel-F bucket. The bucket had been calibrated independently at the same field and temperature. The raw data for **8** were corrected for the molecular diamagnetism. The diamagnetic contribution of the complex **8** was measured from an analogous diamagnetic metal complex **7** [2]. The details of the diamagnetic corrections made can be found in Ref. [7].

2.6. Spectroscopy

ESR spectra were measured on an X-band Bruker EMX-10 spectrometer equipped with an Oxford Instruments liquid helium cryostat. Magnetic field values were measured with a digital counter. The X-band resonator was a dual-mode cavity (Bruker ER 4116 DM). Proton and ^{13}C NMR spectra were recorded at 599.95 and 150.87 MHz, respectively, on Varian Unity Inova-600 spectrometers locked on deuterated solvent and referenced to the solvent peak. Proton NMR is relative to CD_2Cl_2 or $CDCl_3$ at $\delta = 5.30$ or 7.24 and ^{13}C NMR to the center line of CD_2Cl_2 or $CDCl_3$ at $\delta = 53.6$ or 77.0. HMQC (heteronuclear multiple quantum coherence) was used to correlate protons and carbon through one-bond coupling and HMBC (heteronuclear multiple bond coherence) for two- and three-bond proton–carbon coupling. Nuclear Overhauser effect (NOE) difference spectroscopy was employed to determine the ^1H–^1H proximity through space over a distance of up to about

Table 2
Selected bond distances (Å) and angles (°) for compounds **4**·$C_6H_5CH_3$, **5**·0.6$CHCl_3$, **6**·$C_6H_5CH_3$ and **8**·CH_2Cl_2·MeOH.

Compound ***4***·$C_6H_5CH_3$			
Bond lengths (Å)			
Zn–N(1)	2.032(2)	Zn–N(5)	1.963(2)
Zn–N(2)	1.935(2)		
Zn–N(3)	2.064(2)		
Bond angles (°)			
Zn–N(5)–N(4)	97.9(2)	N(1)–Zn–N(2)	94.9(1)
N(2)–Zn–N(5)	153.2(1)	N(1)–Zn–N(3)	156.11(9)
N(3)–Zn–N(5)	88.21(9)	N(1)–Zn–N(5)	92.8(1)
		N(2)–Zn–N(3)	94.8(1)
Compound ***5***·0.6$CHCl_3$			
Bond lengths (Å)			
Ni–N(1)	1.927(3)	Ni–N(5)	1.841(3)
Ni–N(2)	1.887(3)	Ni–N(3)	1.946(3)
Bond angles (°)			
Ni–N(5)–N(4)	104(1)	N(1)–Ni–N(2)	94.0(1)
N(2)–Ni–N(5)	164.7(1)	N(1)–Ni–N(3)	165.7(1)
N(3)–Ni–N(5)	87.9(1)	N(1)–Ni–N(5)	87.3(1)
		N(2)–Ni–N(3)	94.1(1)
Compound ***6***·$C_6H_5CH_3$			
Bond lengths (Å)			
Cu–N(1)	2.012(3)	Cu–N(5)	1.914(3)
Cu–N(2)	1.916(3)	Cu–N(3)	1.995(3)
Bond angles (°)			
Cu–N(5)–N(4)	101.4(2)	N(1)–Cu–N(2)	94.4(1)
N(2)–Cu–N(5)	159.3(1)	N(1)–Cu–N(3)	159.5(1)
		N(1)–Cu–N(5)	87.6(1)
N(3)–Cu–N(5)	90.9(1)	N(2)–Cu–N(3)	94.2(1)
Compound ***8***·CH_2Cl_2·MeOH			
Bond lengths (Å)			
Mn–N(1)	2.066(2)	Mn–N(5)	1.872(2)
Mn–N(2)	1.941(2)	Mn–O(1)	1.967(2)
Mn–N(3)	2.068(2)		
Bond angles (°)			
O(1)–Mn–N(1)	111.81(7)	N(1)–Mn–N(5)	88.30(8)
O(1)–Mn–N(2)	93.22(8)	N(2)–Mn–N(3)	90.94(7)
O(1)–Mn–N(3)	103.17(7)	N(2)–Mn–N(5)	178.35(8)
O(1)–Mn–N(5)	88.34(7)	N(3)–Mn–N(5)	88.20(8)
N(1)–Mn–N(2)	91.58(7)	C(45)–O(1)–Mn	128.5(1)
N(1)–Mn–N(3)	144.71(7)	C(51)–N(5)–Mn	136.8(2)

4 Å. Elemental analyses were carried out on an Elementar Vario EL III analyzer.

The positive-ion fast atom bombardment mass spectrum (FAB MS) was obtained in a nitrobenzyl alcohol (NBA) matrix using a JEOL JMS-SX/SX 102A mass spectrometer. UV–vis spectra were recorded at 20 °C on a HITACHI U-3210 spectrophotometer.

2.7. X-ray crystallography

Table 1 presents the crystal data as well as other information for Zn(*N*-NCO(*o*-OH)C_6H_4-tpp)·$C_6H_5CH_3$ (**4**·$C_6H_5CH_3$), Ni(*N*-NCO(*o*-OH)C_6H_4-tpp)·0.6$CHCl_3$ (**5**·0.6$CHCl_3$), Cu(*N*-NCO(*o*-OH)C_6H_4-tpp)·$C_6H_5CH_3$ (**6**·$C_6H_5CH_3$) and Mn(*N*-NCO(*o*-O) C_6H_4-tpp)·CH_2Cl_2·MeOH (**8**·CH_2Cl_2·MeOH). Measurements were taken on a Bruker AXS SMART-1000 diffractometer using monochromatized Mo Kα radiation (λ = 0.71073 Å) at a temperature of 100(2) K for **8**·CH_2Cl_2·MeOH and 293(2) K for **4**·$C_6H_5CH_3$, **5**·0.6$CHCl_3$ and **6**·$C_6H_5CH_3$. Empirical absorption corrections were made for complexes **4**–**6** and semi-empirical absorption corrections were made for **8**. The structures were solved by direct methods (SHELXL-97) [9] and refined by the full-matrix least-squares method. The (*o*-OH)BA group within **5**·0.6$CHCl_3$ is disordered with an occupancy factor of 0.85 for Cl(1) Cl(2) Cl(3) and 0.15 for Cl(1) Cl(2) Cl(3). The solvate within **6**·$C_6H_5CH_3$ is disordered with an occupancy factor of 0.5 for C(53) and 0.5 for C(53).The Mn atom and the solvent CH_2Cl_2 within **8**·CH_2Cl_2·MeOH is disordered with an occupancy factor of 0.63 for Cl(1)Cl(2) and 0.37 for Cl(1)Cl(2), 0.91 for Mn and 0.09 for Mn. All non-hydrogen atoms were refined with anisotropic thermal parameters, whereas all hydrogen atoms were placed in calculated positions and refined with a riding model. The solvent toluene has been refined in Zn (II) complex of **4**, hence its empirical formula is

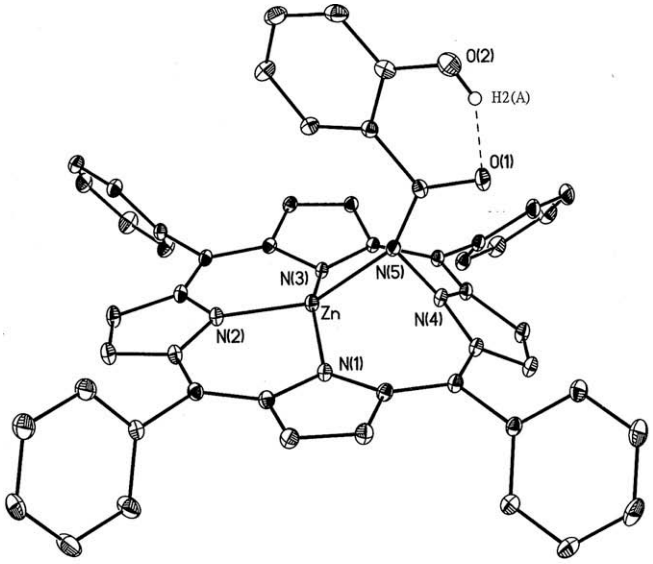

(a) **4**·$C_6H_5CH_3$

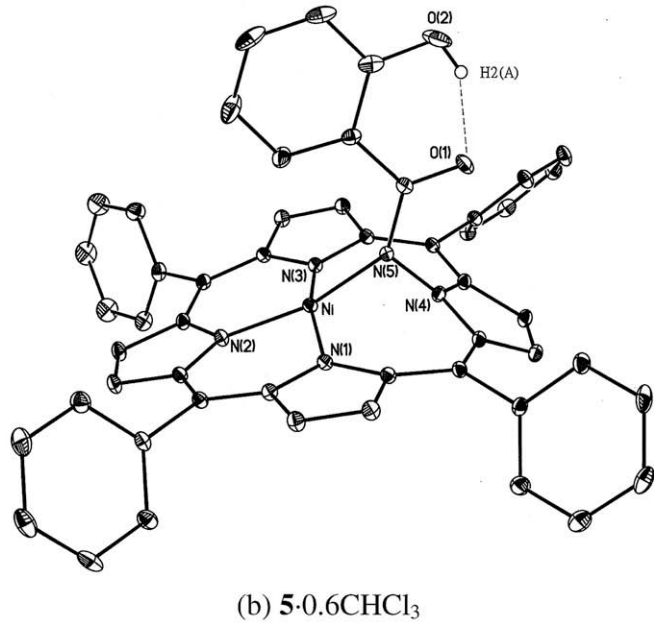

(b) **5**·0.6$CHCl_3$

Fig. 2. (a) Molecular structures of [Zn(*N*-NCO(*o*-OH)C_6H_4-tpp)·$C_6H_5CH_3$; **4**·$C_6H_5CH_3$] and (b) [Ni(*N*-NCO(*o*-OH)C_6H_4-tpp)·$CHCl_3$; **5**·0.6$CHCl_3$], with 30% thermal ellipsoids. Hydrogen atoms, solvent $C_6H_5CH_3$ for **4**·$C_6H_5CH_3$ and solvent $CHCl_3$ for **5**·0.6$CHCl_3$ are omitted for clarity.

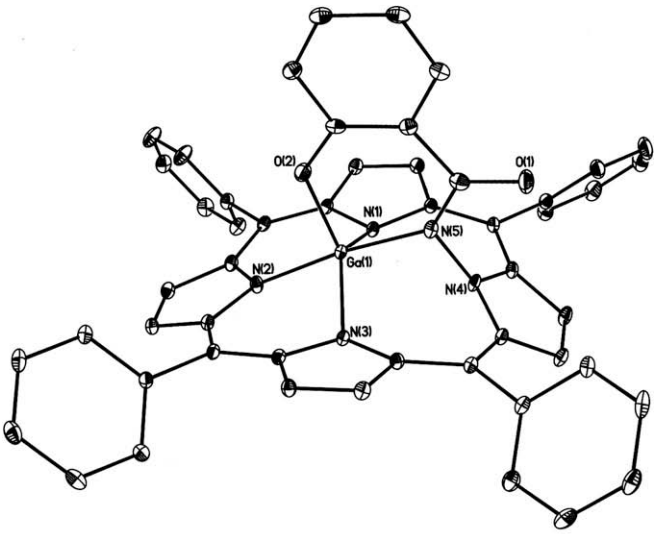

(a) **7**·0.5$CHCl_3$·MeOH

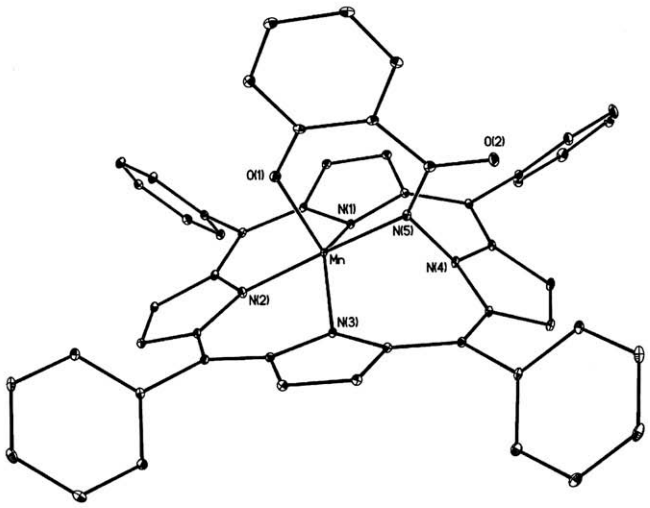

(b) **8**·CH_2Cl_2·MeOH

Fig. 3. (a) Molecular structures of [Ga(*N*-NCO(*o*-O)C_6H_4-tpp)·0.5$CHCl_3$·MeOH; **7**·0.5$CHCl_3$·MeOH] [2] and (b) [Mn(*N*-NCO(*o*-O)C_6H_4-tpp)·CH_2Cl_2·MeOH; **8**·CH_2Cl_2·MeOH], with 30% thermal ellipsoids. Hydrogen atoms, solvent $CHCl_3$ and MeOH for **7**·0.5$CHCl_3$·MeOH and solvent CH_2Cl_2 and MeOH for **8**·CH_2Cl_2·MeOH are omitted for clarity.

$C_{58}H_{41}N_5O_2Zn$. Moreover, the eight hydrogen atoms in solvent toluene are not refined in Cu (II) complex of **6**, hence its empirical formula is $C_{58}H_{33}CuN_5O_2$. Table 2 lists selected bond distances and angles for complexes **4**·$C_6H_5CH_3$, **5**·0.6$CHCl_3$, **6**·$C_6H_5CH_3$, and **8**·CH_2Cl_2·MeOH.

3. Results and discussion

3.1. Structures of 4–6, 8

The X-ray framework is depicted in Fig. 1b for **6**, in Fig. 2 for complexes **4** and **5** and in Fig. 3 for complexes **7** and **8** (Figs. S1–S3 in Supplementary data) [2]. All these structures, four-coordinate, distorted square planar (DSP) geometrical zinc of **4** (or nickel of **5**, copper of **6**) and five-coordinate gallium of **7** (or manganese of **8**) have bonding with three nitrogen atoms of the porphyrins and one extra nitrogen atom of the nitrene fragment in common but compounds **7** and **8** have in addition one more O^- [(*o*-O)BA-Ph] ligand in the axial site. The metal-ligand bond distances and the angles are summarized in Table 2.

The distortion in five-coordinate complex **8** can be quantified by the "degree of trigonality" which is defined as $\tau = (\beta - \alpha)/60$, where β is the largest and α the second largest of the L_{basal}–M–L_{basal} angles [10]. The limiting values are $\tau = 0$ for an ideal tetragonal geometry and $\tau = 1$ for an ideal trigonal bipyramid. In the present case, we find $\beta = 178.35(8)$ [N(5)–Mn–N(2)] and $\alpha = 144.71(7)$ [N(1)–Mn–N(3)] for **8**·CH_2Cl_2·MeOH. Thus τ values calculated for **8**·CH_2Cl_2·MeOH is 0.56. This τ value is close to that of 0.57 for **7** [2]. Hence the geometries around Mn(III) in **8**·CH_2Cl_2·MeOH are best described as a distorted trigonal bipyramid (DTBP) (or a square-based pyramidally distorted trigonal bipyramid, SBPDTBP) with O(1) N(1), and N(3) lying in the equatorial plane for **8**·CH_2Cl_2·MeOH [11].

We adopt the plane of the three strongly bound pyrrole nitrogen atoms [i.e., N(1), N(2) and N(3)] as a reference plane 3N for **4**–**8**. The benzamide nitrogen N(5) in **4**–**8** is located considerably far from the 3N plane. In **4**–**6**, Zn^{2+} (or Ni^{2+}, Cu^{2+}) and N(5) are located on the same sides at 0.35 (or 0.18, 0.30) and 1.53 (or 0.84, 1.24) Å from its 3N plane for complexes **4**(or **5**, **6**), respectively. In **7**–**8**, Ga^{3+} (or Mn^{3+}) and N(5) are also located on the same sides at 0.67 (or 0.58) and 1.11 (or 1.09) Å from its 3N plane for **7** (or **8**), respectively (Table 3) (Fig. S5 in Supplementary data) [2]. The N(4) pyrrole rings bearing the BA group in **4**–**8** could deviate mostly from the 3 N plane, orienting separately in a dihedral angle of 36.4° (or 41.3°, 30.4°) for **4** (or **5**, **6**) and of 37.5° (or 38.6°) for **7** (or **8**) (Table 3) [2].

3.2. Intramolecular hydrogen bonding

Hydrogen bonding results in downfield shifts of proton resonances from their positions in the unbounded state. The low-field values of phenols at δ 11.18–11.95 ppm for **3**, **4** and **5** are attributed to intramolecular hydrogen bonding (Table 3). Intramolecular hydrogen bonding in **3**, **4** and **5** involves the nonbonding electron of the carbonyl oxygen. As a result, the carbonyl carbon that becomes more positive, led to a deshielding of about 4.7 ppm from 162.8 ppm for **7** to 166.0–168.2 ppm for **3**, **4** and **5** (Table 3) [2].

3.3. ESR studies

Complex **6** is paramagnetic because of the d^9 configuration of Cu(II). The unpaired electron resides in the $d_{x^2-y^2}$ orbital, which leads to characteristic ESR spectra for **6** in $CHCl_3$ at 20 °C: four peaks due to the nuclear spin ($I = 3/2$) of the Cu and a nine-line pattern due to the super hyperfine interactions with the four nitrogens ($I = 1$) of the porphyrin. The ESR spectra are typical for planar copper (II) complex with $g_{iso} = 2.04$, A_{iso} (^{63}Cu) = 85.7 G, and A_{iso} (^{14}N) = 12.6 G for **6** in CH_2Cl_2 at 20 °C and with $g_{||} = 2.19$ and $A_{||}$ (^{63}Cu) = 179.4 G for **6** in CH_2Cl_2 at 77 K (Fig. S4 in Supplementary data). These hyperfine couplings are similar in magnitudes to those of $g_{iso} = 2.086$, A_{iso} (^{63}Cu) = 86.5 G and A_{iso} (^{14}N) = 14.4 G obtained from Cu(OETPP) in CH_2Cl_2 solution at 298 K [12].

The X-band (9.426 GHz) ESR spectrum using parallel polarization recorded for **8** in powder solid at 20 °C is shown in Fig. 4. As has been similarly observed in other Mn(III) complexes, the single line centered at ~814 G is found. This signal is attributed to a forbidden transition within the $|2^+\rangle$ and $|2^-\rangle$ non-Kramber's doublet for the high-spin mononuclear Mn^{3+} (S = 2) complex (Fig. 4) [13].

3.4. Magnetic properties

A single band for the absorption spectrum of **8** is found to occur at 463.9 nm. With the band assignment $^5E_g \rightarrow {}^5T_{2g}$ we then get Dq = 2156 cm^{-1} for **8**. Magnetic data for complex **8** are reported in Fig. 5 in the forms of χ_M and μ_{eff} versus *T*. As can be seen in Fig. 5, the value of μ_{eff} varies from 4.50 μ_B at 300 K to 3.81 μ_B at 2 K. The magnetic moment clearly shows a plateau equal to 4.50 μ_B at high temperature (300–30 K), below which it rises slowly to 4.52 μ_B at 20 K before decreasing again. The abrupt rise in μ_{eff} in the range $2 < T < 20$ K is characteristic of compound **8** with significant zero-field splitting (ZFS). The room-temperature effective moment of 4.50 μ_B is lower than the spin-only moment of 4.9 μ_B

Table 3
^1H, ^{13}C NMR (20 °C), X-ray data and *Z* values for complexes **3**–**8**.

Compounds	r_{ion} (Å)	X-ray				^1H NMR (*o*-OH) BA-Ph (ppm) OH	^{13}C NMR (*o*-OH) BA (ppm) BA–CO	*Z* [d] [6]	Classification of metal ions[e][6]
		Δ(3N) [a] (Å)	M···O(2)[b] [or Mn^{3+}···O(1)] (Å)	θ[c] (°)	Coordination geometry				
Cu^{2+} in **6**	0.71	0.30	5.639	36.4	DSP[f]			0.177	B
Ni^{2+} in **5** (in CD_2Cl_2)	0.63	0.18	5.677	41.3	DSP	11.18	168.2	0.293	B
Zn^{2+} in **4** (in CD_2Cl_2)	0.74	0.35	5.707	30.4	DSP	11.49	166.0	0.656	B
3 (in $CDCl_3$)[2]				28.6		11.95	168.2		
Ga^{3+} in **7** (in $CDCl_3$)[2]	0.69	0.67	1.880(4)	37.5	DTBP[g]		162.8	1.167	E
Mn^{3+} in **8**	0.72	0.58	1.9666(16)	38.6	DTBP			1.698	E

[a] Δ(3N) denotes the displacement of the metal center from the 3N plane.
[b] M = Zn^{2+},Ni2+, Cu^{2+}, Ga^{3+}.
[c] θ: dihedral angle between the pyrrole ring bearing a (*o*-OH)BA group and the 3N plane.
[d] *Z*: Zhang's scale for strengths of Lewis acids [6].
[e] Electrostatic or covalent nature of Lewis acids. B acids = border acids, E acids = large electrostatic acids [6].
[f] DSP = distorted square planar.
[g] DTBP = distorted trigonal bipyramid.

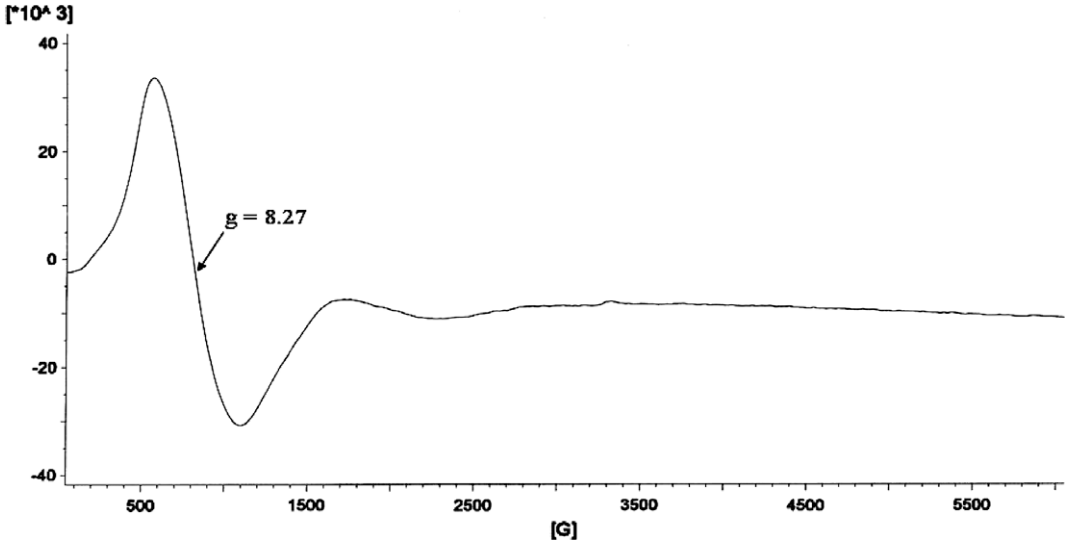

Fig. 4. X-band ESR spectra for the powder sample of **8** at 293 K: parallel polarization. ESR conditions: microwave frequency of 9.426 GHz (parallel polarization), microwave power of 19.971 mW, magnetic field modulation amplitude of 1.60 G and modulation frequency of 100.00 KHz.

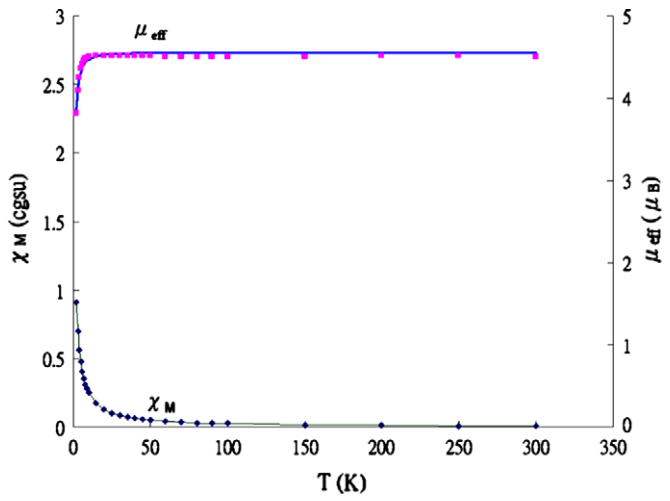

Fig. 5. Temperature variation of the molar magnetic susceptibility (χ_m) and effective magnetic moment (μ_{eff}) for the powder sample of **8** in the range 2–300 K. Points represent the experimental data; solid lines represent the least-squares fit of the data to Eq. (1).

for an S = 2 system, but consistent with that of other high-spin Mn(III) complex in which $g < 2$ [14–16]. The χ_M versus T (or μ_{eff} versus T) data could be fit into the expression (i.e. eq. (1)) derived from the Hamiltonian $\hat{H} = D[S_z^2 - \frac{1}{3}S(S+1)] + E(S_x^2 - S_y^2) + g\mu_B HS$, where H is the applied magnetic field, g is the g tensor, $S = 2$ is the electronic spin and D and E are the parameters which describe the effects of axial and rhombic ligand field, respectively [17]. In **8**, the molecule has an effective C_s symmetry with a mirror plane running through the N(2)–Mn–N(5)–N(4) unit and hence we set $E = 0$. The data were inserted into the Bleaney–Bowers equation (Eq. (1)) [8,17],

$$\bar{\chi}_M = \frac{0.3749}{T} g^2 \frac{1}{3}\left[\frac{8 + 2e^{3y} + \frac{1}{y}\left(-\frac{8}{3} - \frac{28}{3}e^{3y} + 12e^{4y}\right)}{2 + 2e^{3y} + e^{4y}}\right] \quad (1)$$

where $y = 1.44\frac{D(\mathrm{cm}^{-1})}{T}$.

Here g is the average g value and other symbols have their standard meanings. The best fits as represented in Fig. 5 gave the values of $g = 1.86$ and $|D| = 3.0\ \mathrm{cm}^{-1}$. This value lies near the $1 < |D| < 4.9\ \mathrm{cm}^{-1}$ range found in related Mn(III) porphyrin complexes [12]. We do not succeed in coordinating the Hg^{2+} (C acid, $Z = -1.063$), Tl^{3+} (C acid, $Z = -0.580$) and Cd^{2+} (C acid, $Z = -0.108$) ions into ligand **3**.

4. Conclusion

Compound **3** has thus been shown to coordinate in a tetrafunctional manner with Zn(II) (B acid), Ni(II) (B acid) and Cu(II) (B acid) and pentafunctional manner with Ga(III) (E acid) and Mn(III) (E acid). We have investigated these four new porphyrin metal complexes, namely two paramagnetic **6** and **8**, and two diamagnetic **4** and **5** and their X-ray structures are established. The conventional ESR spectroscopy and the magnetic susceptibility measurements were reported to evaluate the ZFS parameter D for the high-spin mononuclear Mn(III) ($S = 2$) of **8**.

Acknowledgements

The financial support from the National Science Council of the R.O.C. under Grant NSC 95-2113-M-005-014-MY3 is gratefully acknowledged. We thank Dr. S. Elango for helpful discussions.

Appendix A. Supplementary data

CCDC 743906, 743907, 743908, and 743909 contains the supplementary crystallographic data for **4**·$C_6H_5CH_3$, **5**·0.6$CHCl_3$, **6**·$C_6H_5CH_3$ and **8**·CH_2Cl_2·MeOH. These data can be obtained free of charge via http://www.ccdc.cam.ac.uk/conts/retrieving.html, or from the Cambridge Crystallographic Data Centre, 12 Union Road, Cambridge CB2 1EZ, UK; fax: (+44) 1223-336-033; or e-mail: deposit@ccdc.cam.ac.uk. Supplementary data associated with this article can be found, in the online version, at doi:10.1016/j.poly.2009.09.009.

References

[1] C.Y. Chen, H.Y. Hsieh, J.H. Chen, S.S. Wang, J.Y. Tung, L.P. Hwang, Polyhedron 26 (2007) 4602.
[2] C.H. Cho, T.Y. Chien, J.H. Chen, S.S. Wang, J.Y. Tung, Personal communication.
[3] H.J. Callot, B. Cheorier, R. Weiss, J. Am. Chem. Soc. 100 (1978) 4733.

[4] R.M. Silverstein, F.X. Webster, D.J. Kiemle, Spectroscopic Identification of Organic Compounds, 7th ed., John Wiley & Sons, New York, 2005. p. 153.
[5] Y. Zhang, Inorg. Chem. 21 (1982) 3886.
[6] Y. Zhang, Inorg. Chem. 21 (1982) 3889.
[7] R.S. Drago, Physical Methods for Chemists, 2nd ed., Saunders College Publishing, New York, 1992. p. 473, 591.
[8] B. Bleaney, K.D. Bowers, Proc. R. Soc. Lond. A 214 (1952) 451.
[9] G.M. Sheldrick, SHELXL-97. Program for Refinement of Crystal Structure from Diffraction Data, University of Gottingen, Gottingen, Germany, 1997.
[10] A.W. Addison, T.N. Rao, J. Reedijk, J.V. Rijn, G.C. Verschoor, J. Chem. Soc., Dalton Trans. (1984) 1349.
[11] R.G. Garvey, R.O. Koob, M.L. Morris, Acta Crystallogr. C 43 (1987) 2056.
[12] M.W. Renner, K.M. Barkigia, Y. Zhang, C.J. Medforth, K.M. Smith, J. Fajer, J. Am. Chem. Soc. 116 (1994) 8582.
[13] S.L. Dexheimer, J.W. Gohdes, M.K. Chan, K.S. Hagen, W.H. Armstrong, M.P. Klein, J. Am. Chem. Soc. 111 (1989) 8923.
[14] M.L. Yates, A.M. Arif, J.L. Manson, B.A. Kalm, B.M. Burkhart, J.S. Miller, Inorg. Chem. 37 (1998) 840.
[15] B.J. Kennedy, K.S. Murray, Inorg. Chem. 24 (1985) 1552.
[16] K.J. Franz, S.J. Lippard, J. Am. Chem. Soc. 120 (1998) 9034.
[17] S.W. Hung, F.A. Yang, J.H. Chen, S.S. Wang, J.Y. Tung, Inorg. Chem. 47 (2008) 7202.